EGU General Assembly 2024
Vienna, Austria & Online | 14–19 April 2024

Session HS7.4 – Steps towards future hydroclimatic scenarios for water resources management in a changing world

Past and future changes of streamflow in the European Alps

Rui Guo[1], Hung T. T. Nguyen[2], Stefano Galelli[2,3], Serena Ceola[1] and Alberto Montanari[1]

1 Department of Civil, Chemical, Environmental and Materials Engineering (DICAM), University of Bologna, Bologna, Italy (Corresponding: rui.guo2@unibo.it)

2 Tree Ring Laboratory, Lamont-Doherty Earth Observatory, Columbia University, Palisades, New York, USA

3 School of Civil and Environmental Engineering, Cornell University, Ithaca, New York, USA.

Introduction

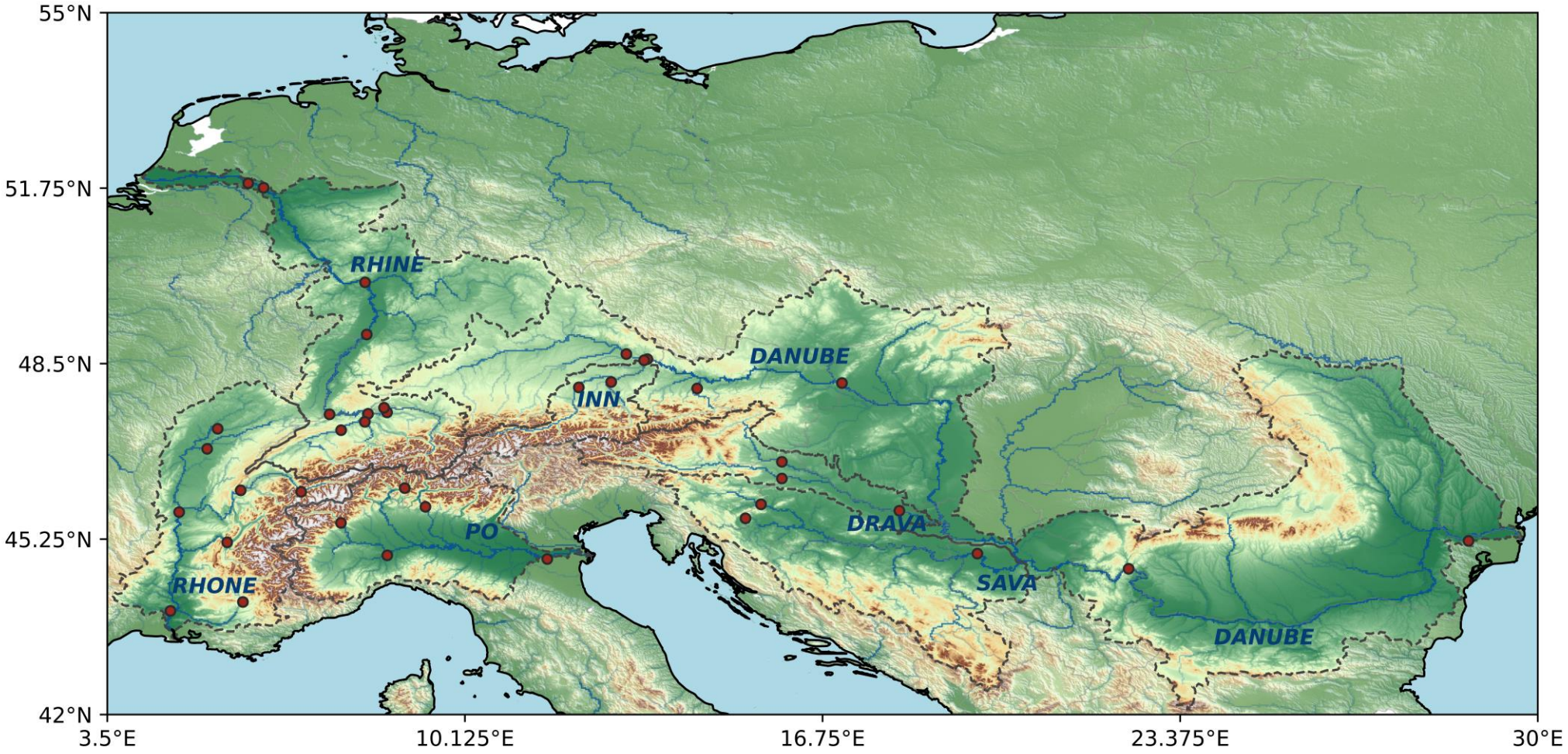

What are the characteristics of long-term variability of streamflow in major rivers in the European Alps and how will it change in the future?

Introduction

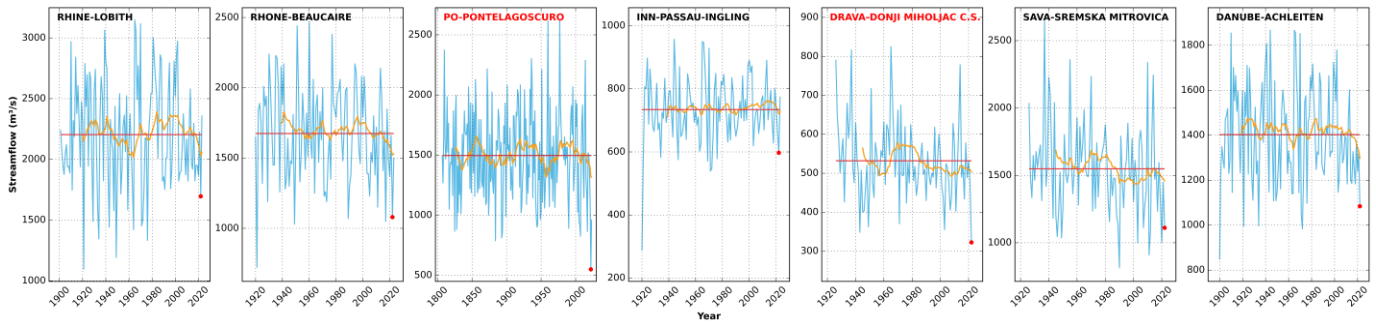

Two basins faced record-breaking event in 2022 and several basins reach the driest 20-years since the instrumental history.

Observed decrease of river flow in past 30-years and the long-last general dry period after 2000 in majority basins together with more frequent low flow events in some basins.

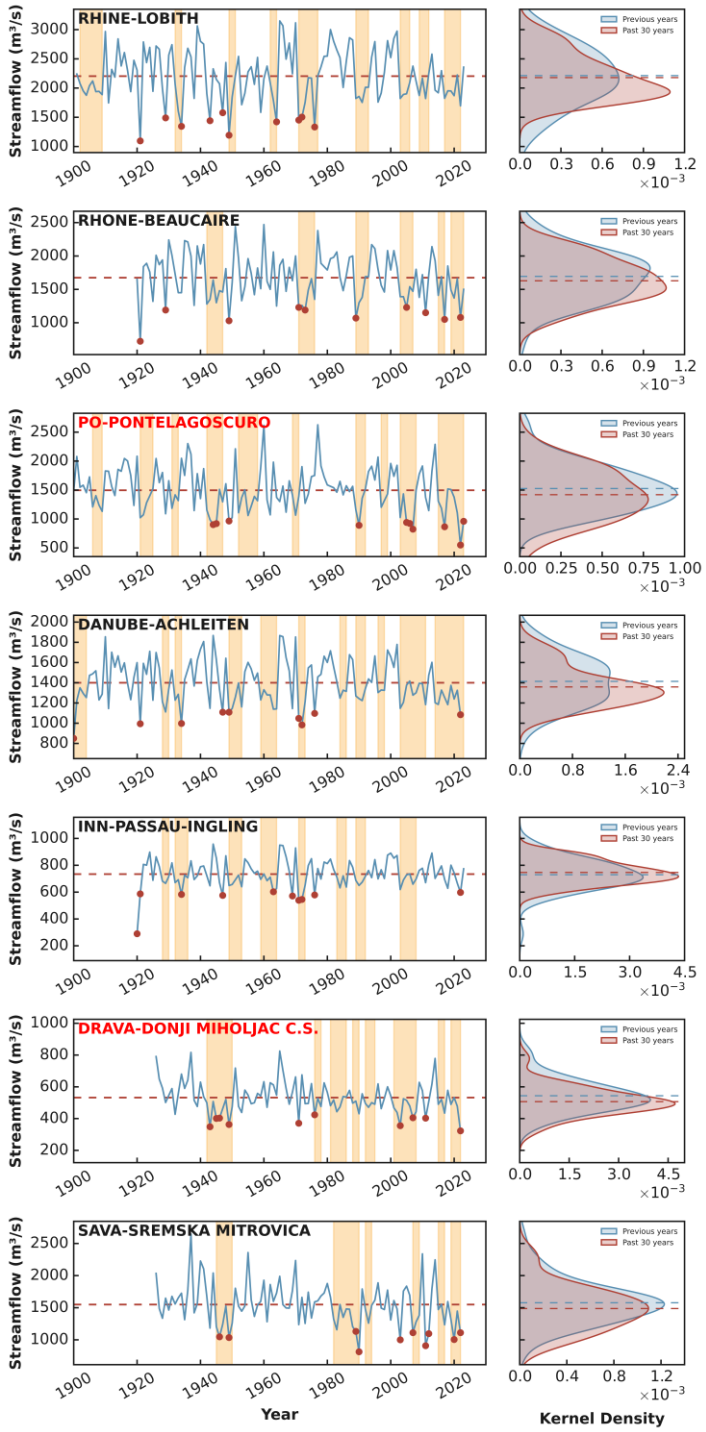

Introduction

- Relatively short instrumental streamflow records limited understanding of the long-term variability in river flow and also rare events such as record-breaking events or multiyear droughts.

- Tree rings, with annual resolution and precise dating, can provide temporally high-resolution proxy records of past climate to reconstruct past streamflow. General Circulation Models (GCMs) are frequently applied in climate studies to simulate the past climate and predict the future climate.

- The main tasks of this study are to (i) reconstruct the streamflow of rivers originated from European Alps in past nine centuries, (ii) evaluate the ability of up-to-date GCMs and our reconstructions in simulating the statistics of observed long-term streamflow by focusing on multiyear hydrological droughts and (iii) to infer how streamflow and drought risk was like in the past and how will it changes in the future.

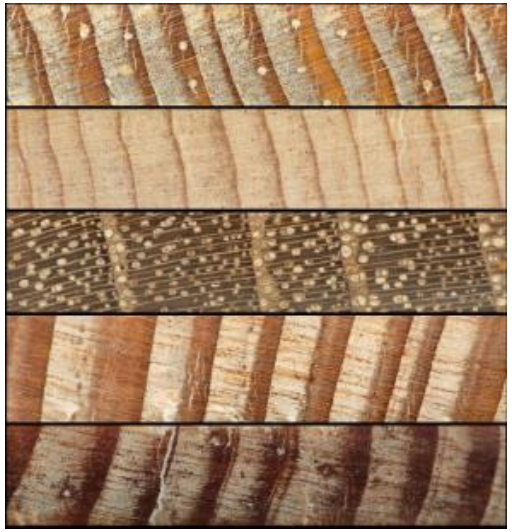

Image for tree cores. Image source: Hung et al. (2022)

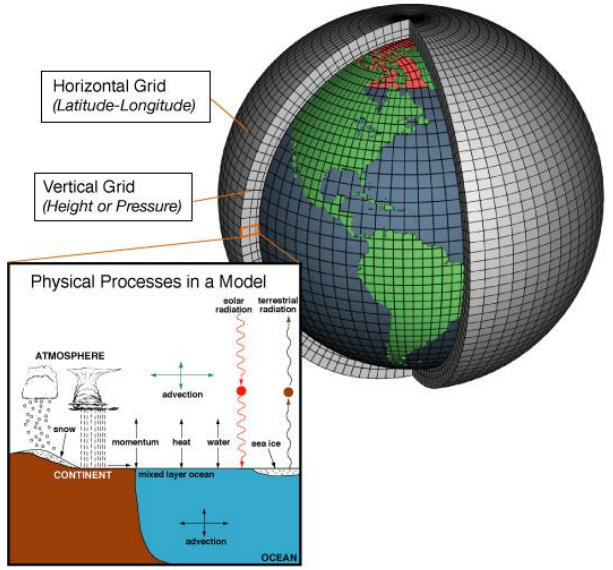

Grid representation of the climate system by GCMs. Processes that are reproduced include physical and chemical phenomena. Image source: NOAA.

Nguyen, Hung TT, et al. "Droughts, Pluvials, and Wet Season Timing Across the Chao Phraya River Basin: A 254-Year Monthly Reconstruction From Tree Ring Widths and δ18O." Geophysical Research Letters 49.17 (2022): e2022GL100442.

Old World Drought Atlas as proxy data

Reasons for choosing OWDA as proxy data:

1. Both streamflow and PDSI can be modeled as functions of ring width, one can build a model to relate streamflow to PDSI directly.

2. Drought atlases offer evenly distributed grid cells and have been systematically corrected. The dataset generally has the same time span for most grid cells, which takes less computational cost for large-scale streamflow reconstruction.

3. Many of the underlying tree ring data are unpublished and thus not accessible

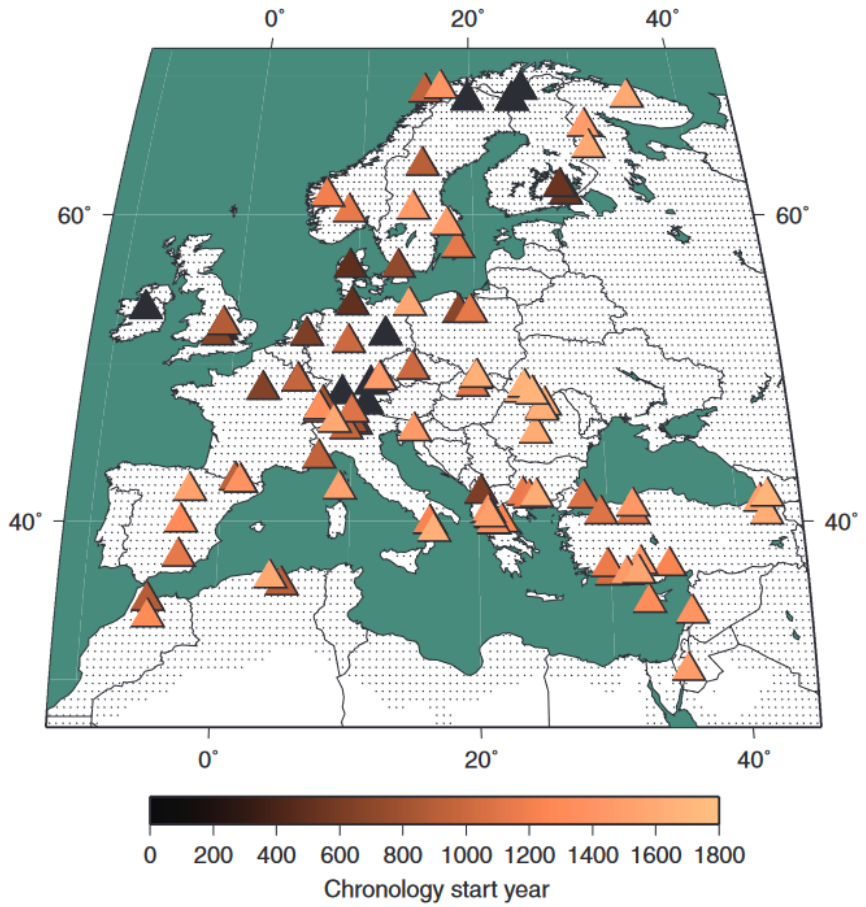

Fig. 1. Map of the JJA scPDSI target field (small black grid points) and the 106 chronology tree-ring network used for reconstruction. There are 5414 half-degree scPDSI grid points. The OWDA tree-ring network (filled triangles shaded by start year) illustrates the reasonably uniform coverage of chronologies across the domain, except for Russia.

Cook et al. (2005) Old World Megadroughts and Pluvials During the Common Era. Science Advances, 1 (10): 110.

Climate-informed proxy Selection

The hydroclimate at a location is characterized by three indices: aridity (a), moisture seasonality (s), and snow fraction (f) for a global $0.5° \times 0.5°$ resolution follow the hydroclimate characterization system (Knoben et al., 2018).

The hydroclimatic similarity between two locations i and j is defined as their Euclidean distance in the hydroclimate space. This distance is termed the KWF distance and its mathematical definition is:

$$d_{KWF}(i,j) = \sqrt{(a_i - a_j)^2 + (s_i - s_j)^2 + (f_i - f_j)^2}$$

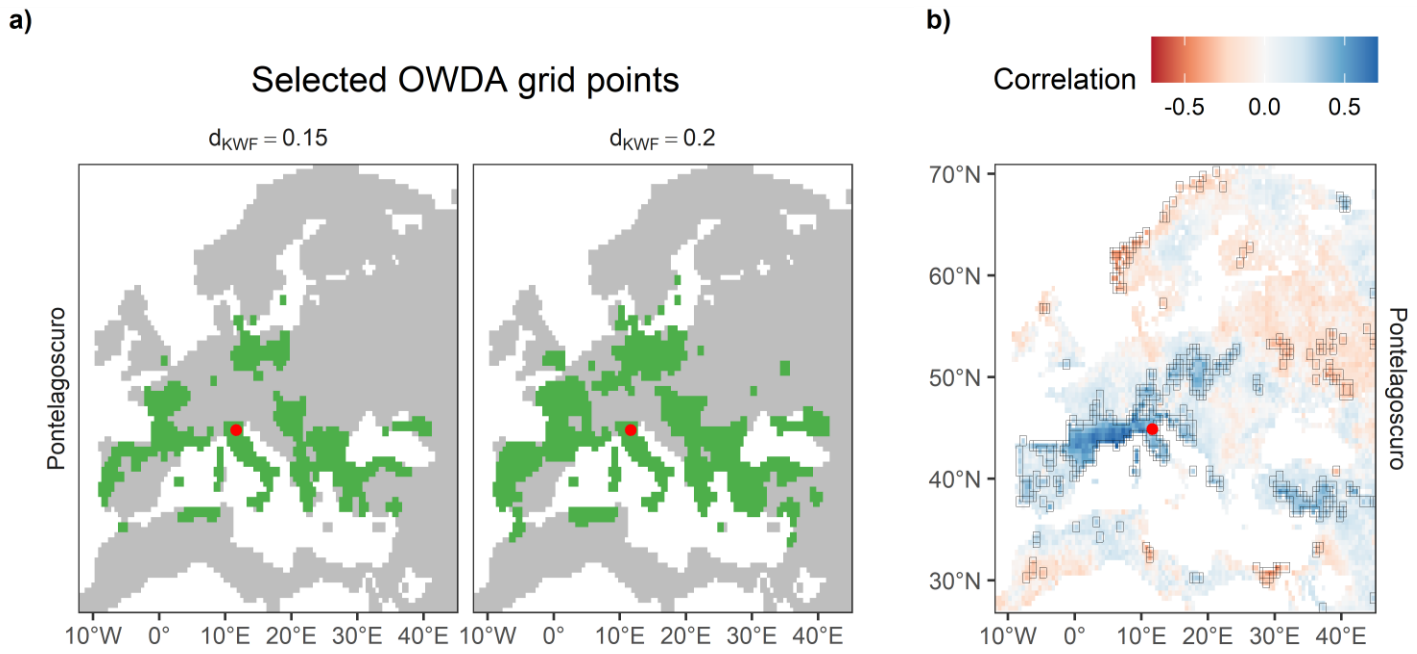

Knoben et al. A quantitative hydrological climate classification evaluated with independent streamflow data, Water Resources Research, 54, 5088–5109, 2018.

ALMA MATER STUDIORUM
UNIVERSITÀ DI BOLOGNA

Reconstruction and Cross-validation

- Weighted principal component analysis (PCA) to remove multicollinearity among the OWDA grid points. We weighted each grid point by its correlation with the target streamflow, using Equation:

$$z_i = g_i \times r_i^p$$

We used the weight exponent p = 0, 0.5, 2/3, 1, 1.5, and 2.

- Performed PCA on z_i and retained only those principal components (PCs) having eigenvalue at least 1.0.

- Selected a subset that is most relevant to the streamflow target using the VSURF (Variable Selection Using Random Forest) algorithm (Genuer et al., 2010).

- Build a linear regression model between the selected PCs and streamflow by using the reconstruction algorithm in the R package ldsr (Nguyen et al., 2020).

- We use a leave-25%-out cross-validation scheme. Three goodness-of-fit statistics, i.e., (1) Reduction of Error (RE), (2) Nash-Sutcliffe Coefficient of Efficiency (CE or NSE), and (3) Kling-Gupta Efficiency(KGE) were selected.

Genuer et al. Variable selection using random forests, Pattern recognition letters, 31, 2225–2236, 2010.
Nguyen et al. Coherent streamflow variability in monsoon Asia over the past eight centuries—Links to oceanic drivers, Water Resources Research, 56, e2020WR027 883, 2020.

GCMs data information

We obtained the runoff output in the spatial domain of the Po River Basin from a 25-model ensemble of phase six of the Coupled Model Intercomparison Project (CMIP6) and a 4-model ensemble of phase four of the Paleo climate Model Intercomparison Project (PMIP4).

https://climate.copernicus.eu/
https://esgf-node.llnl.gov/search/cmip6/

Model	Institution	Resolution	Grid (lon × lat)
ACCESS-CM2	Commonwealth Scientific and Industrial Research Organization- Australian, Research Council Centre of Excellence for Climate System Science, Australia	1.875° × 1.250°	192 × 144
BCC-CSM2-MR	Beijing Climate Center, Beijing, China	1.125° × 1.250°	320 × 160
CanESM5-CanOE	Canadian Centre for Climate Modelling and Analysis, Environment and Climate Change Canada, Canada	2.81° × 2.81°	128 × 64
CESM2	National Center for Atmospheric Research, Climate and Global Dynamics Laboratory, USA	1.25° × 0.94°	288 × 192
CIESM	Department of Earth System Science, Tsinghua University, Beijing, China	1.25° × 0.94°	288 × 192
CMCC-CM2-SR5	Fondazione Centro Euro-Mediterraneo sui Cambiamenti Climatici, Italy	1.25° × 0.94°	288 × 192
CMCC-ESM2	Fondazione Centro Euro-Mediterraneo sui Cambiamenti Climatici, Italy	1.25° × 0.94°	288 × 192
CNRM-CM6-1-HR	Centre National de Recherches Meteorologiques, France	$T359^1$	181724
CNRM-CM6-1	Centre National de Recherches Meteorologiques, France	$T127^2$	24572
CNRM-ESM2-1	Centre National de Recherches Meteorologiques, France	$T127$	24572
EC-Earth3-Veg-LR	Consortium of European Research Institution and Researchers, Europe	1.125° × 1.125°	320 × 160
HadGEM3-GC31-LL	Natural Environment Research Council, UK	1.875° × 1.250°	192 × 144
INM-CM5-0	Institute for Numerical Mathematics, Russian Academy of Science, Russia	2.00° × 1.50°	180 × 120
IPSL-CM6A-LR	Institut Pierre Simon Laplace, Paris, France	2.50° × 1.25°	144 × 143
KIOST-ESM	Korea Institute of Ocean Science and Technology, Republic of Korea	1.875° × 1.875°	192 × 96
MCM-UA-1-0	Department of Geosciences, University of Arizona, USA	3.75° × 2.5°	96 × 80
MIROC6	Japan Agency for Marine-Earth Science and Technology, Japan	1.40° × 1.40°	256 × 128
NorESM2-LM	Norwegian Climate Centre, Norway	2.5° × 1.875°	144 × 96
NorESM2-MM	Norwegian Climate Centre, Norway	1.25° × 0.94°	288 × 192
TaiESM1	Research Center for Environmental Changes, Taiwan, China	1.25° × 0.94°	288 × 192
UKESM1-0-LL	Met Office Hadley Centre, UK	1.875° × 1.250°	192 × 144
INM-CM4-8*	Institute for Numerical Mathematics, Russian Academy of Science, Russia	2.00° × 1.50°	180 × 120
MIROC-ES2L*	Japan Agency for Marine-Earth Science and Technology, Japan	1.40° × 1.40°	256 × 128
MPI-ESM1-2-LR*	Max Planck Institute for Meteorology, Germany	1.875° × 1.875°	192 × 96
MRI-ESM2-0*	Meteorological Research Institute, Japan	1.125° × 1.125°	320 × 160

[1]: Gaussian Reduced with 181724 grid points in total distributed over 360 latitude circles (with 720 grid points per latitude circle between 32.2degN and 32.2degS reducing to 18 grid points per latitude circle at 89.6degN and 89.6degS).
[2]: Gaussian Reduced with 24572 grid points in total distributed over 128 latitude circles (with 256 grid points per latitude circle between 30degN and 30degS reducing to 20 grid points per latitude circle at 88.9degN and 88.9degS).
*: Four models which attend PMIP4 that also provide paleo simulations (past1000 experiments).

GCMs bias correction – Quantile Delta Mapping

First, we compute the empirical frequency of not exceedance $q_{f(t)}$ of each GCM simulated value $m_{f(t)}$during the future denoted by subscript f period. Then, the relative change in quantiles $\Delta(t)$ of GCM simulated precipitation over two time periods is given by:

$$\Delta(t) = \frac{F_f^{-1}(q_{f(t)})}{F_h^{-1}(q_{f(t)})} = \frac{m_f(t)}{F_h^{-1}(q_f(t))}$$

where F_f and F_h denote the distribution of empirical frequencies of each GCM simulated value $m_{f(t)}$ and $m_{h(t)}$during the future and historical period, respectively.

Then, the bias-corrected value $\hat{o}(t)$ of $q_{f(t)}$is computed by the frequency of not exceedance F_o of the observations during the historical period:

$$\hat{o}(t) = F_o^{-1}(q_f(t))$$

Finally, the bias-corrected GCM simulation $\hat{m}_f(t)$ for the future period is given by:

$$\hat{m}_f(t) = \hat{o}(t) \cdot \Delta(t)$$

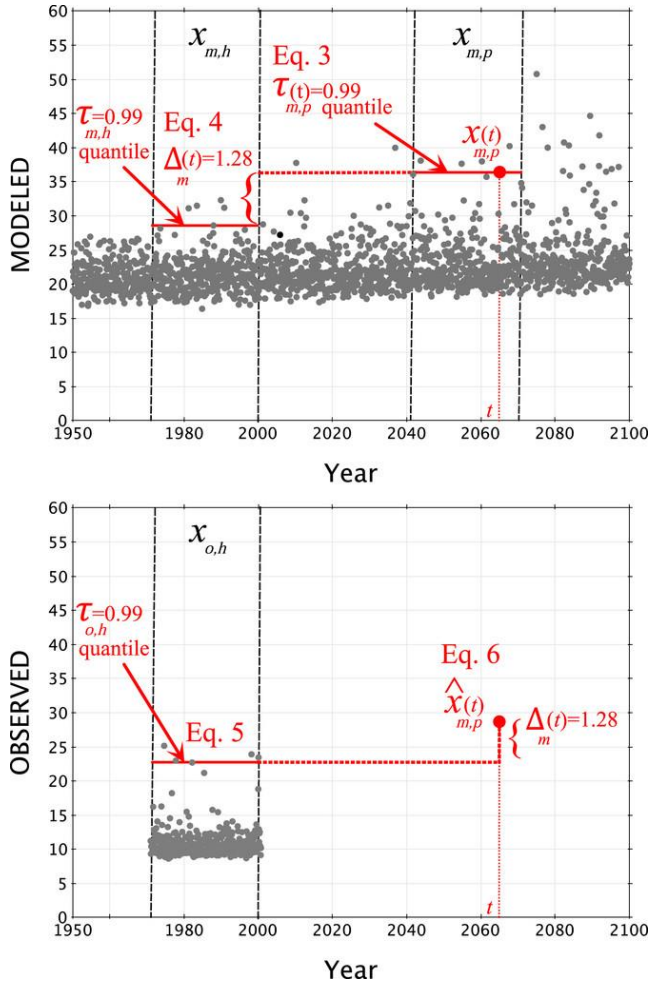

A graphical illustration of the quantile delta mapping algorithm. (Ref: Cannon et al., 2015), DOI: https://doi.org/10.1175/JCLI-D-14-00754.1

ALMA MATER STUDIORUM
UNIVERSITÀ DI BOLOGNA

Drought definition – Run Theory

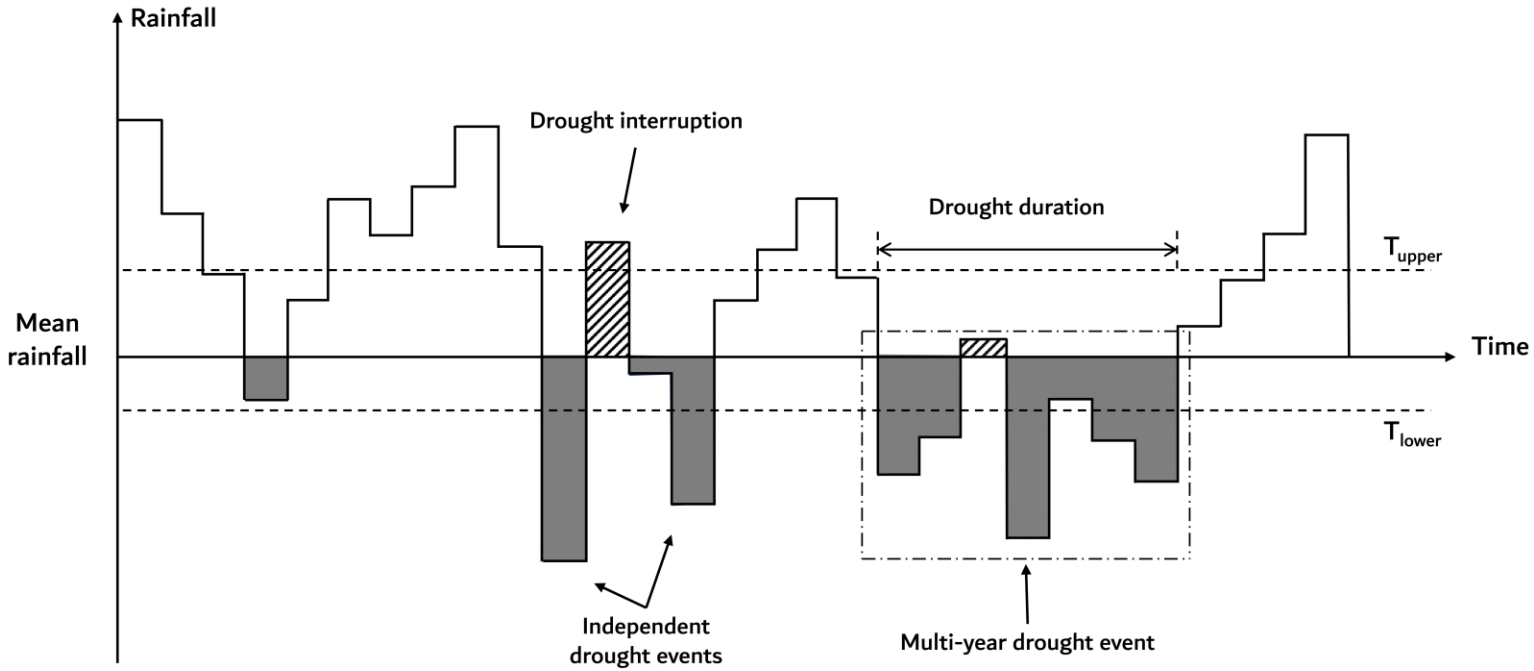

$$Drought\ intensity = \frac{Drought\ severity}{Drought\ duration}$$

Max deficit is the max water scarcity during a drought event.

Streamflow reconstruction skills

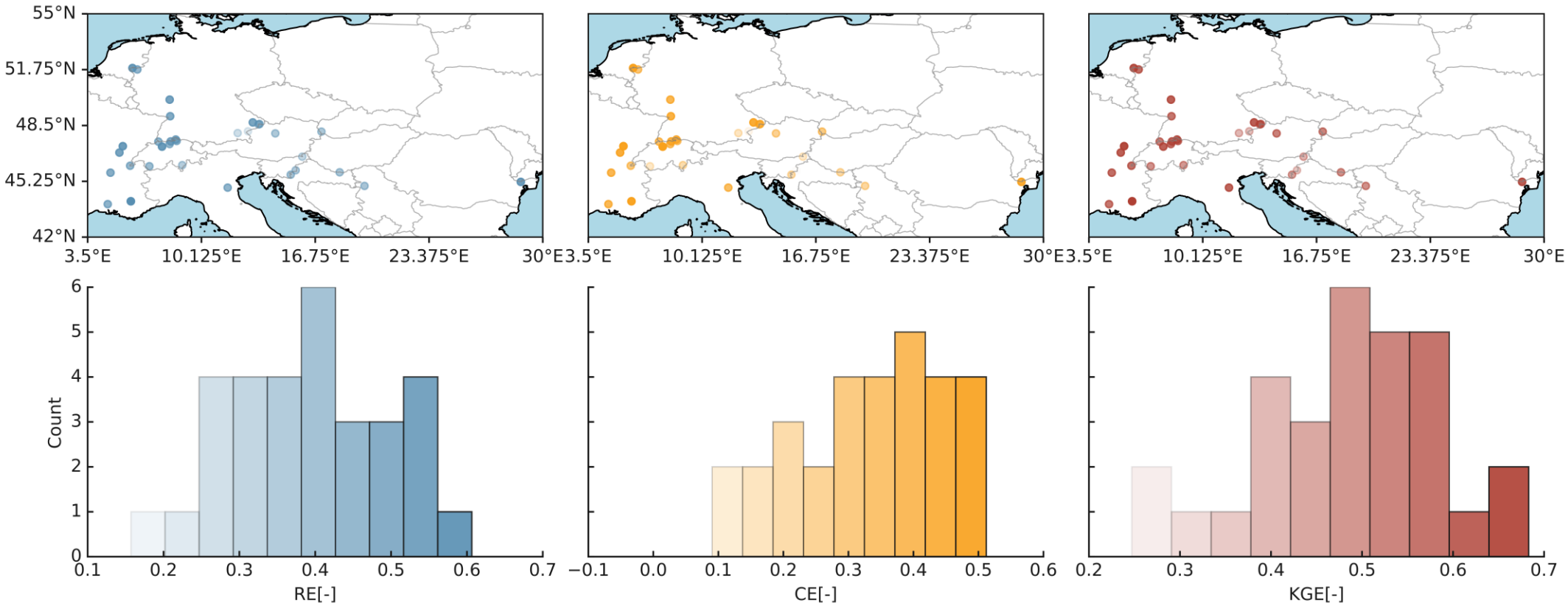

Our reconstruction demonstrates satisfactory performance during cross-validation for statistic metrices.

General good performance for outlets of four major basins (Po, Rhine, Rhone and Danube), but relatively poor performance for the tributaries of Danube (Inn, Sava and Drava).

Streamflow reconstruction skills

Our reconstructions effectively capture the long-term mean river flow and accurately replicates multi-year drought events identified in observational data.

For the low flow events, our reconstructions also show skill in replicating the magnitude while even the time for some events.

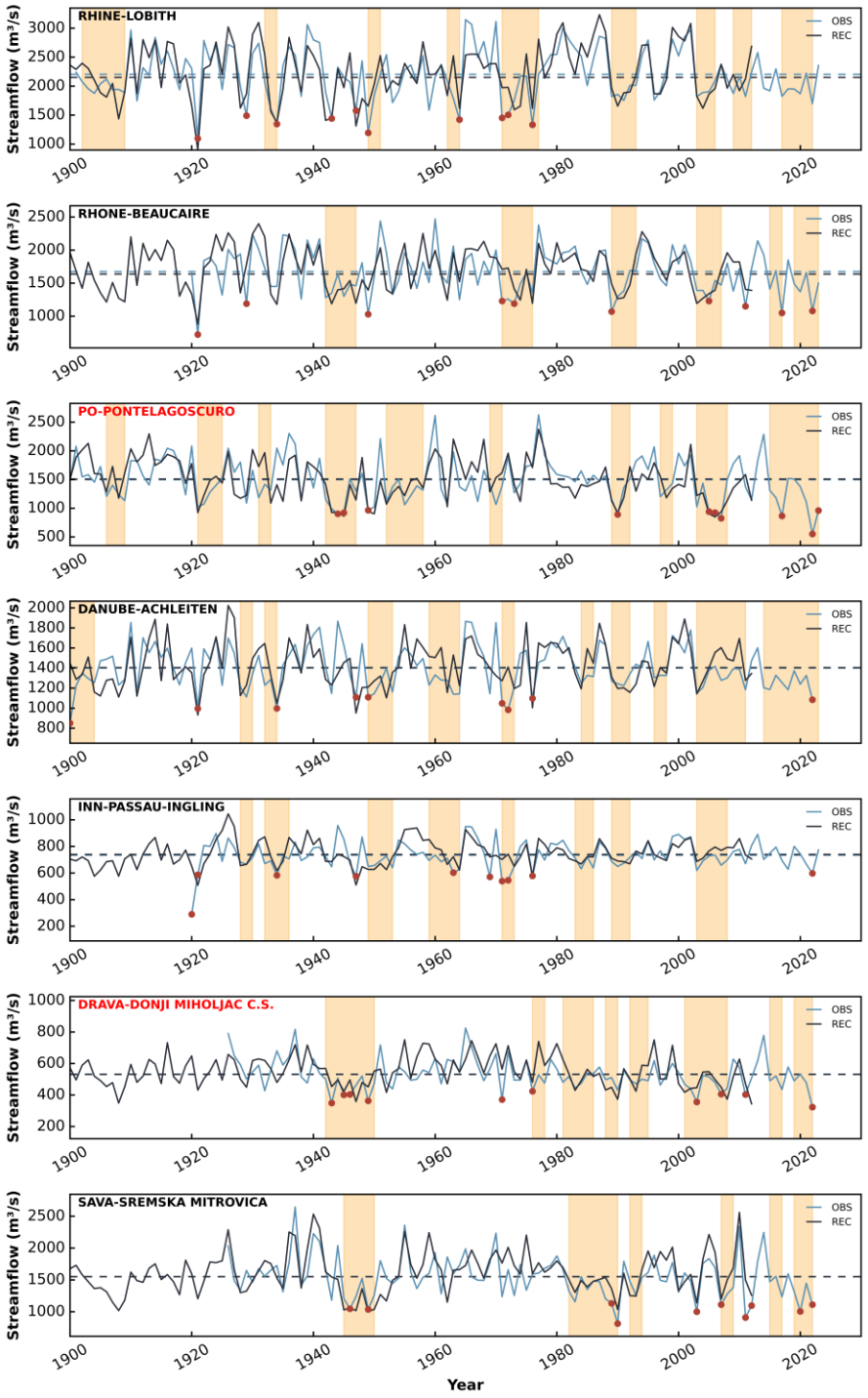

Streamflow variability from past to the future

Long-last drought and high-flow period has occurred in the past.

Coherent dry periods such as during late Medieval Climate Anomaly (MCA), Renaissance and late Little Ice Age for major rivers in Europe.

The most extreme low flow event during instrumental period seems the worst in past 900 years.

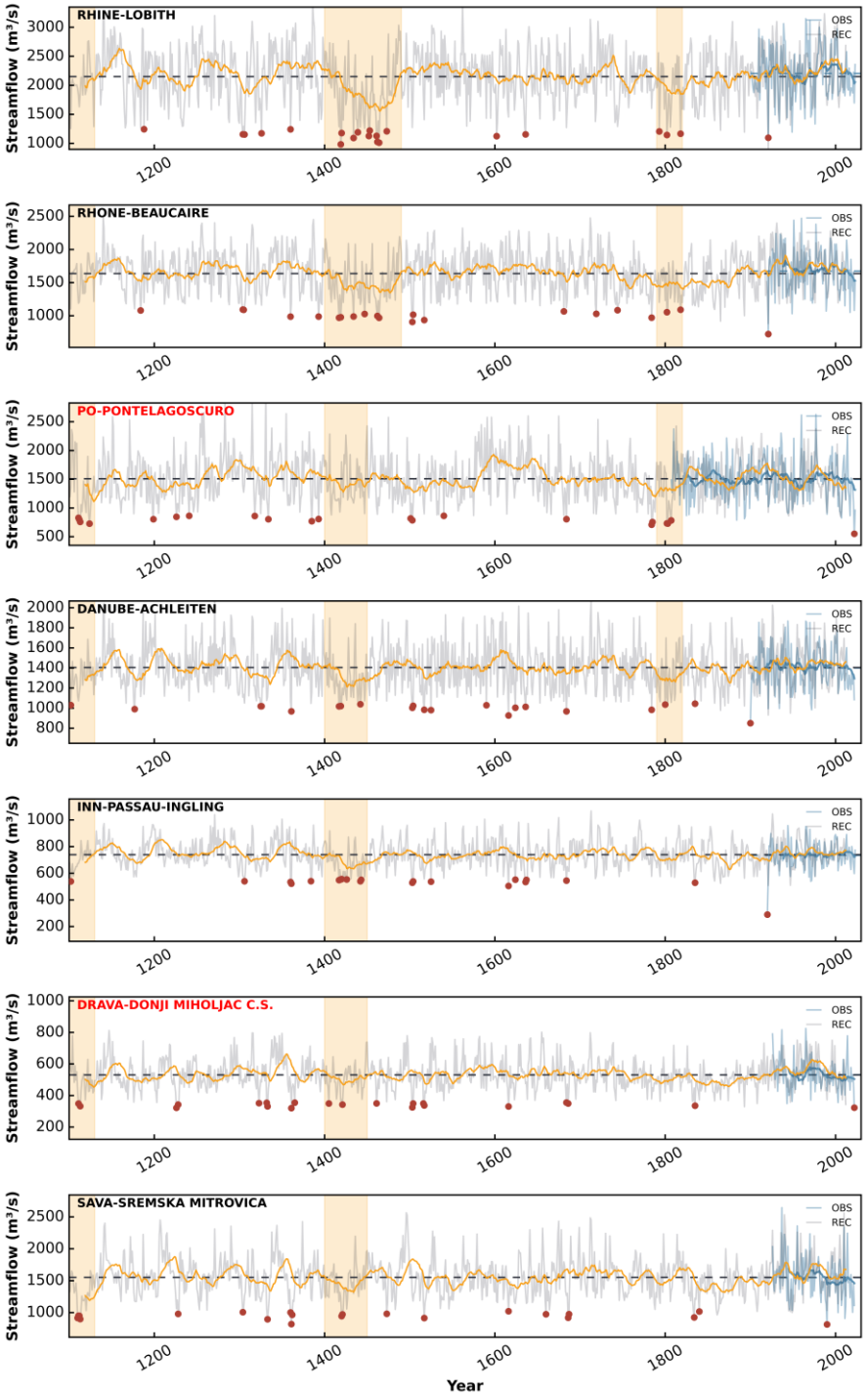

Streamflow variability from past to the future

Similar performance for PMIP4 paleo simulations with respect to our reconstructions.

CMIP6 consistently project a declining trend in the future, surpassing even the most arid condition of our reconstruction and paleo simulations.

This suggests the possibility of unprecedented drought conditions for majority basins in Europe occurring by the end of the 21st century.

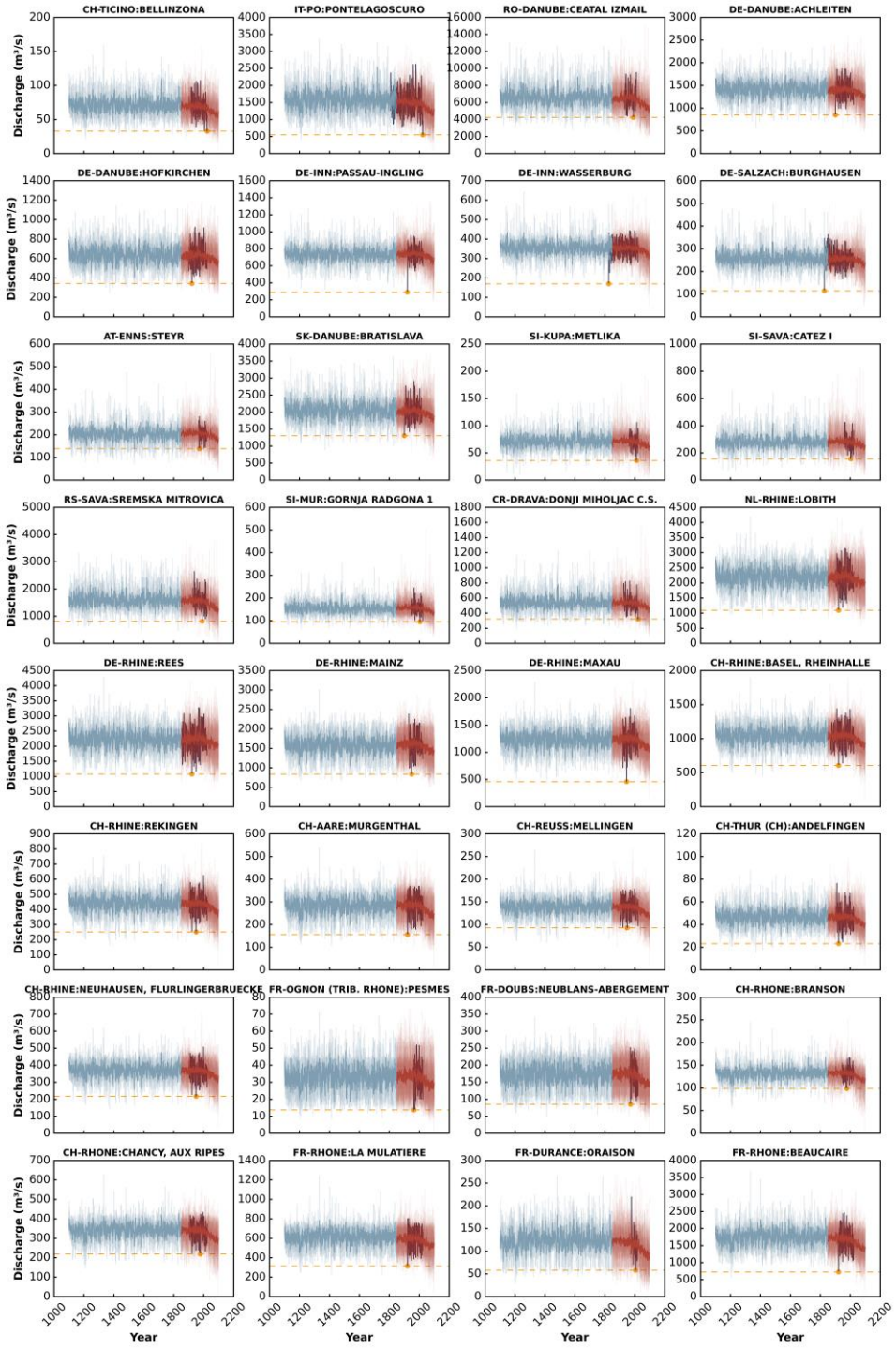

Conclusions

- Our reconstructions for the past nine centuries streamflow of the rivers originated in the European Alps show general good statistic performance during cross-validation period, especially, the outlets of four major basins depict satisfactory performance. Moreover, they well replicate the observed multi-year drought events and some low flow events.

- By looking into the whole time span of reconstructions, the most extreme annual drought events in all basins seem to reach the worst in the past 900 years. However, coherent dry periods which are much longer are identified such as during late Medieval Climate Anomaly (MCA), Renaissance and late Little Ice Age for major rivers in the European Alps .

- Both GCMs and REC well capture the long-term mean annual streamflow. Furthermore, GCMs consistently project a declining trend of mean streamflow in the future, surpassing even the most arid condition of our reconstructions and paleo simulations. This suggests the possibility of unprecedented drought conditions occurring by the end of the 21st century for major rivers in the European Alps.

Thanks for your time and attention!!

ALMA MATER STUDIORUM
UNIVERSITÀ DI BOLOGNA